 https://doi.org/10.3311/PPci.22179


**Periodica Polytechnica Civil Engineering**, 67(3), pp. 902–913, 2023

# Prediction of Rock Tensile Strength Using Soft Computing and Statistical Methods

Jinhuo Zheng[1], Minglong Shen[1,2*], Mohammad Reza Motahari[3*], Mohammad Khajehzadeh[4]

[1] Fujian Architectural Design and Research Institute Co., Ltd.; No. 188, Tonghu Road, Gulou District, Fuzhou, 350001, China
[2] Beijing Jiaotong University, School of Civil Engineering: No. 3 Shangyuan village, Haidian district, Beijing, 100044, China
[3] Department of Civil Engineering, Faculty of Engineering, Arak University, 3848177584 Arak, Iran
[4] Department of Civil Engineering, Anar Branch, Islamic Azad University, 7741943615, Anar, Iran
* Corresponding author, e-mail: minglongshen@stu.cuz.edu.cn; m_motahari@araku.ac.ir

Received: 08 March 2023, Accepted: 03 May 2023, Published online: 16 May 2023

**Abstract**

The tensile strength of the rocks is one of the effective factors in the rupture of structure foundations and underground spaces, the stability of rocky slopes, and the ability to drill and explode in rocks. This research was conducted to estimate tensile strength using methods such as simple regression (SR), multivariate linear regression (MVLR), support vector regression (SVR) with radial basis kernel function, multilayer feed-forward artificial neural network (MFF-ANN), Gaussian process regression (GPR) using squared exponential kernel (SEK) function, and adaptive neuro-fuzzy inference system (ANFIS) based on Gaussian membership function. For this purpose, petrography, and engineering features of the limestone, sandstone, and argillaceous limestone samples in the south of Iran, were assessed. The results obtained from this study were compared with those of previous research, revealing a strong correlation ($R^2$ = 0.95 to 1.00) between our findings and the published works. To estimate Brazilian tensile strength (BTS), the index properties including water absorption by weight, point load index (PLI), porosity%, P-wave velocity (Vp), and density were considered as inputs. Methods were compared using various criteria. The SVR precision (R = 0.96) was higher than MFF-ANN (R = 0.92), ANFIS (R = 0.95), GPR (R = 0.945), and MVLR (R=0.89) to estimate the tensile strength. The average BTS measured in the laboratory and predicted by all 5 methods is 6.62 and 6.71 MPa, respectively, which shows the very high precision of the investigated methods. Analysis of model criteria using statistical analysis for developed relationships revealed that there is sufficient accuracy to use the empirical equations.

**Keywords**

geo-mechanical features, intelligent methods, statistical analysis, prediction, sedimentary rocks

## 1 Introduction

Tensile strength is a basic parameter of intact rock when designing and constructing engineering structures on rocks. This parameter controls the stability of the underground mines and galleries, the stability of rocky slopes, the ability to drill, and also the design of blasting in rocks. Mineralogy, the nature and intensity of the bond between the particles or the type and amount of cementation, and the porosity, density, and water absorption of the rock affect the tensile strength [1, 2]. The limitations of laboratory conditions and the difficulties of preparing a suitable sample for this experiment have led various researchers to use intelligent and statistical approaches to predict the tensile strength of the rocks [3, 4].

The diverse mineralogical composition, textural properties, and physical characteristics of sandstones make them susceptible to weathering and degradation [5, 6]. The resistance of these rocks to weathering is influenced by the mineralogical composition, type and percentage of cement, porosity, particle size, permeability, and the joints [3]. Properties such as durability, crystal size, dolomitization processes (conversion of calcite mineral to dolomite), grain size, density, porosity, and hardness degree control the strength of the carbonates [7]. Researchers have used regression analysis for estimating the tensile strength using nondestructive experiments (Table 1). Arman [8] assessed the relationships between tensile strength and uniaxial compressive strength of the rocks using regression analysis. Also, Armaghani et al. [9] used statistical analysis to estimate the BTS. Mahdiyar et al. [10] predicted BTS of rocks using various intelligent methods. Huang et al. [11] used MVLR and MFF-ANN to estimate tensile strength of the rock samples. Baykasoğlu et al. [12] used genetic pro-

**Cite this article as:** Zheng, J., Shen, M., Motahari, M. R., Khajehzadeh M. "Prediction of Rock Tensile Strength Using Soft Computing and Statistical Methods", Periodica Polytechnica Civil Engineering, 67(3), pp. 902–913, 2023. https://doi.org/10.3311/PPci.22179

**Table1** Previous relationships for predicting BTS

| Empirical relationships | $R^2$ | Rock type | Researchers |
|---|---|---|---|
| BTS = 1.1PLI + 1.25 | 0.82 | Sandstone | Mishra and Basu [21] |
| BTS = 3.34PLI – 3.4 | 0.90 | Various rock | Karaman et al. [22] |
| BTS = 1.57PLI + 1.514 | 0.52 | Various rock | Yilmaz [23] |
| BTS = 0.79PLI - 0.38 | 0.56 | Sedimentary rocks | Khajevand and Fereidooni [24] |
| BTS = 0.005Vp – 8.36 | 0.84 | Various rocks | Singh et al. [13] |
| BTS = 7.51Ln(PLI) + 2.22 | 0.93 | Various rocks | Kiliç and Teymen [25] |
| BTS = 1.050Vp1.389 | 0.75 | Various rocks | Karakul and Ulusay [26] |
| BTS = 0.0015Vp – 0.3164 | 0.64 | Granite rocks | Parsajoo et al. [2] |
| BTS = 0.45Vp1.87 | 0.92 | Various rocks | Kiliç and Teymen [25] |
| BTS = 1.132PLI + 3.008 | 0.67 | Granite rocks | Harandizadeh et al. [4] |

gramming approach to estimate the tensile strength of the limestone rocks. In addition, Parsajoo et al. [2] employed intelligent techniques to determine the BTS of the rocks. Singh et al. [13] forecasted the BTS of various rocks by MFF-ANN and statistical methods. Also, Fattahi and Hasanipanah [14] and Hasanipanah et al. [15] estimated BTS using machine learning methods. Dao et al. [16] used MFF-ANN and GPR to estimate the compressive strength of the concrete samples. Jahed Armaghani et al. [17] predict rock brittleness using the SVM. Also, Mahmoodzadeh et al. [18] predict rock quality designation (RQD) using several methods and stated that the GPR achieves better than other methods. Lawal et al. [19] utilized GPR, ANN, and response surface method (RSM) to forecast rock mechanical properties based on P-wave and rock density. The findings indicated that GPR yielded more precise outcomes than the ANN and RSM methods. Acar and Kaya [20] assessed the effect of tensile strength on the elastic modulus of the weak rocks.

The key purpose of the current study was for predicting the BTS of sedimentary rocks to save on expensive tests such as BTS, and to evaluate the influence of mineralogy on geotechnical characteristics by porosity, PLI, density, water absorption (Wa), and Vp using MFF-ANN, ANFIS, GPR, SVR, SR, and MVLR. Samples were collected from 11 operational mines located in Bushehr province, primarily comprising sandstone, travertine, and limestone extracted from the Mishan and Aghajari formations (Table 1) [2, 4, 21–25].

## 2 Materials and methods

### 2.1 Laboratory tests

To carry out this study, rock blocks were selected and transported to the laboratory, where they were prepared for laboratory experiments [27]. The collected blocks must be free of any joints, cracks, and weathering effects to prevent the effect of anisotropy on geomechanical results. Cylindrical specimens were prepared, and a wear device was used to parallel the two ends of the specimens. The prepared cylindrical specimens have a diameter of 54 mm (NX size), and their height-to-diameter ratio is approximately 2. Before BTS and PLI tests, the compressional wave velocity test with the frequency of 0.5 MHz, and physical tests were performed on the samples [27]. The apparent porosity% of the specimens was measured via the method of buoyancy and saturation.

The BTS tests were conducted on specimens with a height-to-diameter ratio of 1:1, as per ASTM [28] standard. The samples were subjected to continuous loading at a constant rate of 200 N/s.

Cylindrical specimens were subjected to the point load index (PLI) test following the ASTM [29] standard. Finally, thin sections were obtained from each specimen and evaluated using the Folk [30] and Dunham [31]

### 2.2 The MFF-ANN

Artificial neural networks (ANNs) can be broadly classified into two categories based on their learning algorithm and topology: feed-forward neural networks (FFNNs) and feed-back neural networks (FBNNs). In a FFNN, the signals flow only in the forward direction. A multilayer feed-forward artificial neural network (MFF-ANN) typically consists of an input layer that receives information, a hidden layer that utilizes a nonlinear activation function, and an output layer that produces the network's output based on the input and hidden layers [8, 32–34].

### 2.3 The SVR

The SVR matches a curve with epsilon ($\varepsilon$) width on the model to obtain the lowest error [17]. Functions such as $f(x) = \boldsymbol{W}.x + b$ are used for predicting in this method ($x$ and $b$ are bias values and $\boldsymbol{W}$ is the weight vector). The appropriate error function is used by SVR to eliminate errors that are within a certain range of real values. As a result, by minimizing the weight vector, the model test error is minimized. Among polynomial, linear, quadratic, and radial kernel functions used in the SVR method, the radial has shown the best efficiency for forecasting rock mechanic problems [17].

### 2.4 The ANFIS

The membership function (MF) value in classical logic is assigned 1 if a member belongs to a set, and 0 if it does not. Conversely, in fuzzy set theory, each member of a fuzzy set may possess an MF value ranging from 0 to 1. This method is commonly referred to as Eq. (1) in mathematical discourse [2].

$$A = \left\{x,; \mu_A(\mathrm{x})\right\} \left| x \in \mathrm{x} \right| \tag{1}$$

The MF degree reflects the extent to which a member is associated with the fuzzy set. Several fuzzy inference systems (FIS) were presented. Two types of FIS such as Sugeno and Mamdani algorithms are commonly used [2]. The difference between the two methods is due to the fuzzy rules used. The FIS is a fundamental rule-based system comprised of a collection of linguistic rules capable of achieving high precision in modeling various systems and serving as a versatile predictor. Fuzzy logic-based rule systems utilize linguistic parameters such as rules and outcomes, where rules can be expressed in terms of inference or non-equality. To demonstrate the capabilities of both neural networks and fuzzy systems, neuro-fuzzy systems (NFS) can be introduced. One of the NFSs that allows fuzzy systems to learn rules with a back-propagation algorithm is ANFIS [2]. In this study, The ANFIS model was trained using the combined method, which entails recursive error propagation and the least squares technique.

### 2.5 The GPR

A Gaussian process (GP) is characterized by a group of random variables that share a common Gaussian distribution. By utilizing the underlying structures within the data, GPR analysis enables effective data classification. Within the GP framework, a distribution function $f$ is defined, which maps the $X$ input space onto the $R$ space [19]. For every finite subset of $X$, the marginal distribution is $p(f(x_1), f(x_2),..., f(x_n))$, which follows a multi-variate normal distribution [18]. In general, GPR coding is based on the assumption that inputs close to each other are likely to have alike outputs, hence, higher weights are assigned to samples with points with similar values.

### 2.6 Normalization of data

Normalization of data is the most common activity in machine learning. Data normalization offers numerous benefits, including better gradient descent efficiency on normalized data compared to abnormal data. Additionally, normalizing input values helps avoid extremely large or small effects on weight. In current research, data was normalized between -1 and 1 using Eq. (2).

$$X_i = 2\left(\frac{X - X_{\min}}{X_{\max} - X_{\min}}\right) - 1\,, \tag{2}$$

where, $X$ is measured value, $X_{\min}$ is the minimum data, and $X_{\max}$ is the maximum data.

### 2.7 Efficiency appraisal of methods

To evaluate the methods, we utilized several metrics including the mean absolute percentage error (MAPE) (Eq. (3)), variance accounted for (VAF) (Eq. (4)), root mean square error (RMSE) (Eq. (5)), and the determination coefficient.

$$\mathrm{MAPE} = \frac{1}{N}\sum_{i=1}^{N}\left|\frac{y - y'}{y}\right| \times 100\,, \tag{3}$$

$$VAF = 100\left[1 - \frac{\mathrm{var}(y - y')}{\mathrm{var}(y)}\right], \tag{4}$$

$$RMSE = \sqrt{\frac{\sum_{i=1}^{N}\left(Measured_i - Predicted_i\right)^2}{N}}\,, \tag{5}$$

where, $y$, $y'$, $N$, and $s^2$ are the measured, estimated, total data, and variance, respectively.

## 3 Results and discussion

### 3.1 Geo-mechanical properties of samples

The values of maximum, minimum, and average geomechanical properties on 66 samples (32 samples of limestone, 14 samples of argillaceous limestone, and 20 sandstone samples) are displayed in Table 2. The mean BTS and PLI are 6.71 MPa and 3.75 MPa, respectively (Table 2). According to the classification of Bieniawski [35], based on the mean of PLI, the samples were classified as the medium category.

The mechanical properties of foundation materials affect the stability of civil and mining structures [36, 37]. Mineralogical and physical properties have a significant effect on the mechanical properties and stability of mines [38]. The type of cement and organic matter, the type and amount of minerals cause changes in the mechanical properties and stability of the slopes [39, 40]. Also, humidity has a significant effect on the engineering properties and stability of structures [41, 42]. Clay minerals cause swelling and instability by absorbing water [41]. These minerals were very few in the studied samples. Rock bursting occurs in deep mines and in quartz-rich

**Table 2** Measured properties on the samples

| Rock types | Statistics | Vp (Km/s) | D (g/cm$^3$) | A (%) | P (%) | BTS (MPa) | PLI (MPa) |
|---|---|---|---|---|---|---|---|
| Limestone | Mean | 5.12 | 2.52 | 5.43 | 7.06 | 9.10 | 5.01 |
| | Minimum | 4.42 | 2.41 | 4.08 | 4.36 | 7.11 | 3.55 |
| | Maximum | 5.79 | 2.63 | 6.75 | 9.00 | 12.50 | 8.00 |
| Sandstone | Mean | 4.13 | 2.38 | 7.40 | 10.12 | 5.33 | 2.87 |
| | Minimum | 3.07 | 2.34 | 6.75 | 9.00 | 2.71 | 2.00 |
| | Maximum | 4.36 | 2.41 | 8.88 | 13.79 | 7.00 | 3.55 |
| Marly limestone | Mean | 2.60 | 2.27 | 9.91 | 15.35 | 1.71 | 1.44 |
| | Minimum | 2.06 | 2.10 | 9.00 | 13.96 | 0.11 | 0.31 |
| | Maximum | 2.99 | 2.32 | 11.00 | 16.72 | 2.60 | 1.94 |

P = Porosity, A = Water absorption, D = Density, PLI = Point load index, BTS = Brazilian tensile strength

rocks [43, 44]. Stress release, cracks and fractures, faults and earthquakes are also involved in the escalation of this phenomenon [45–47]. Because the depth of these mines is less than 45 meters, and the overburden stress is negligible. Hence, the risk of rock bursting has not occurred in the studied mines.

### 3.2 Failure modes of the samples

Examining the types of failure modes during laboratory tests is very important. This study helps to create an understanding of how to create and develop fractures of various types of fractures in rock and more accurate and safer design of the project under different loading conditions. The description of different types of failure modes has been presented by Gurocak et al. [3]. In the BTS test, central (C), non-central (NC), Central with layer activation (C+LA) and central multiple (CM) fracture modes were seen. Triple junction (TJ) and single plane (SP) fracture modes were observed in the point load test. Laboratory works being performed on the samples are depicted in Fig. 1.

### 3.3 Thin section studies

According to microscopic studies, in the classification proposed by Dunham [31], the limestone specimens were categorized in the range of mudstone to grainstone groups (Table 3). The studied sandstones are classified as calclitharenite according to the Folk [30] classification. These rocks consist of carbonaceous rock fragments (26 to 75), volcanic gravel (2 to 35%), metamorphic fragments (2 to 18%), feldspar (1 to 10%), dark minerals (1 to 8%), quartz (0 to 22%), and chert (2 to 11%). Sub-components such as clay and gypsum are also observed in some samples. The types of cement in the samples are gypsum and calcite. The grains of these sandstones are semi-rounded to angular and have medium to poor sorting.

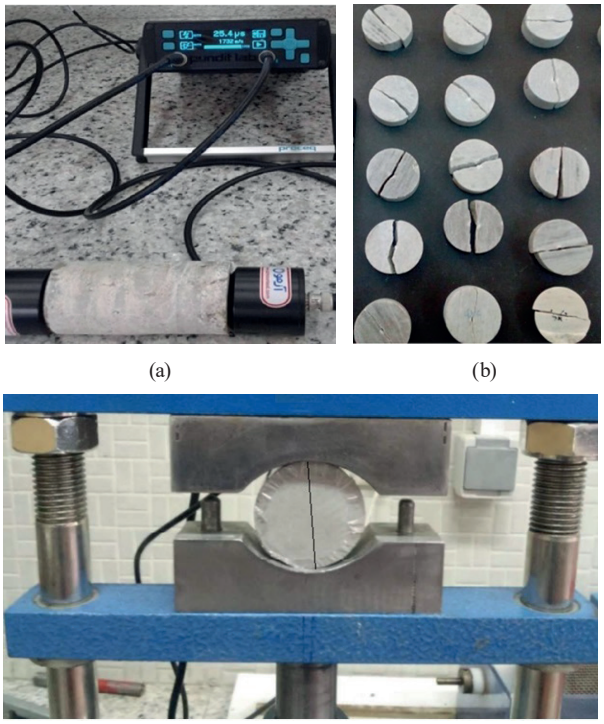

(a) (b)

(c)

**Fig. 1** Some of of lab activities.; a) A sample in Vp test, b) Some samples after point load test, c) A sample in BTS test

**Table 3** Developed relationships between BTS and inputs

| Equations | $R^2$ | RMSE | Eq. No. |
|---|---|---|---|
| BTS = -0.78P + 14.12 | 0.64 | 2.96 | (6) |
| BTS = 2.79Vp – 5.53 | 0.76 | 2.81 | (7) |
| BTS = -1.34A + 15.80 | 0.58 | 2.99 | (8) |
| BTS = 20.86D – 44.10 | 0.50 | 3.21 | (9) |
| BTS = 1.46PLI + 1.23 | 0.54 | 3.91 | (10) |

### 3.4 Texture effect on sample characteristics

Characteristics of sedimentary rocks are more influenced by texture [48]. The studied limestones as a Guri section of Mishan formation are composed of medium to thick

layer limestones with some fossils. These fossils represent the shallow marine environment that was deposited during the Miocene. The texture type of 32 limestone samples includes mudstone (34.37%), wackestone (34.37%), packstone (18.76%), and grainstone (12.50%), respectively. Comparison of tensile strength, compressional wave velocity, point load index, and density of limestone specimens with texture of samples shows that there is an increasing trend in these properties with the texture change from mudstone to grainstone. The results of thin sections on 11 samples of argillaceous limestone showed that there are three types of texture in these samples, and they do not have grainstone texture. According to the Dunham [31] classification, 18.9% of these samples are mudstone, 45.45% wackstone, and 36.36% packstone. For these samples, there was a logical trend between geomechanical properties and texture percentage. By changing the texture from mudstone to packstone, the strength properties increase. The frequency of fossil fragments in this group of samples is higher than the studied limestone and sandstone samples, which has led to a decrease in the resistance of these samples.

### 3.5 Correlation matrix

The correlation matrix and the histogram charts of the variables are shown in Fig. 2. It is observed that there is a good correlation and logical trend between BTS and other properties. As porosity and water absorption increase, there is a decrease in the point load index and tensile strength. The porosity (P) and Vp have the highest effect on BTS (Fig. 2). The results show that samples with higher porosity and water absorption have lower tensile strength because increasing porosity and the presence of water reduce the degree of bonding and entanglement of rock grains, which decreases the tensile strength. Research indicates that the Vp, in comparison to other properties, is more effective at predicting rock strength [13, 25]. In general, Fig. 2 shows that input variables can be used in the modeling process to estimate the BTS of the studied sedimentary rocks. Table 3 shows relationships between BTS and inputs.

### 3.6 Assessing the findings in relation to global research

Many equations have been developed to forecast the BTS of the sedimentary rocks (see Table 1). Here, via the background empirical equations, BTS was predicted for each sample of the 66 samples. Then, the accuracy and data distribution of the estimated BTS with the measured ones were determined (Fig. 3). Comparing the results to previous research reveals a strong correlation between the actual BTS and estimated values based on the relationships established in prior studies. (Fig. 3). Determination coefficient from 95% (for Yilmaz [23] and Parsajoo et al. [2] relationships) to 100% (for Singh et al. [13] relationship) is variable. Hence, relationships related to similar rocks in the present study, have high accuracy with measured data. Hence, it is possible to perform modeling techniques on the data to estimate BTS.

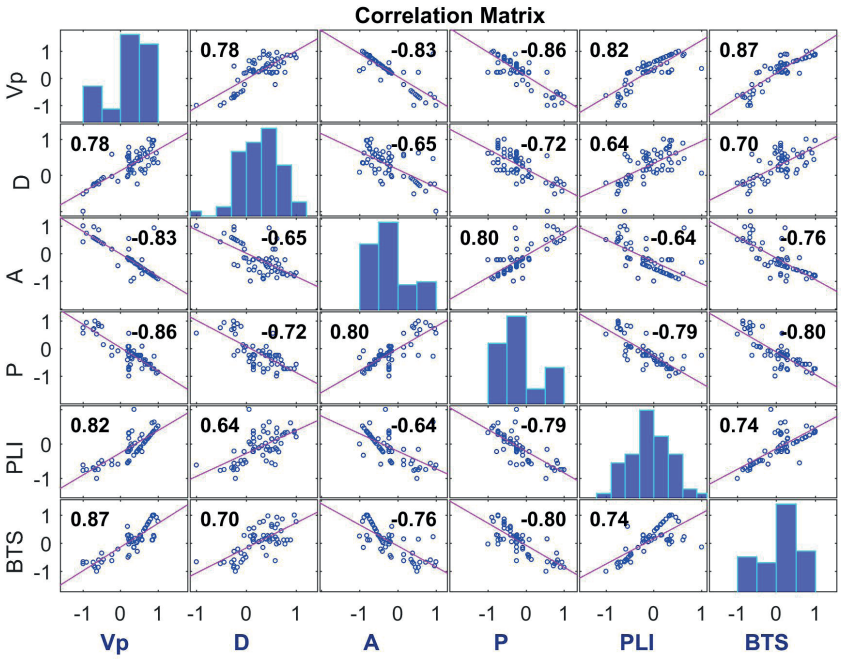


**Fig. 2** Correlation matrix of the variables

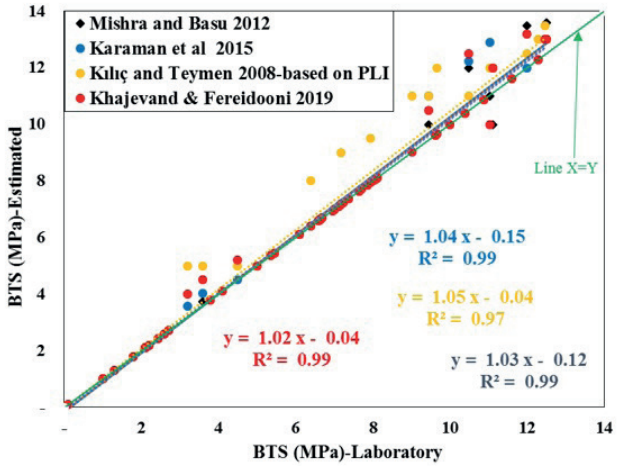


(a)

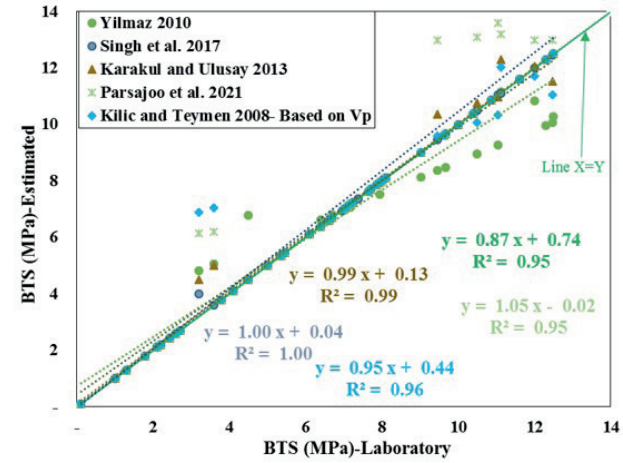


(b)

**Fig. 3** Relationships between predicted BTS (based on previous relationships) and measured values

### 3.7 Multivariate linear regression (MVLR)

The MVLR analysis in this study was conducted using Minitab software, and the resulting equation for predicting BTS using this method is presented in Table 4.

Durbin-Watson statistic (DWS), RMSE, MAPE, and $R^2$ were used to appraise the relationship. The DWS test is utilized to assess the independence of errors in relation to each other, with the acceptable range for DWS falling between 1.5 and 2.5. In this study, this statistical test demonstrates that the errors are independent, indicating that the developed model can be used. Meanwhile, ANOVA is typically utilized to evaluate the accuracy of the regression equation. In this study, ANOVA resulted in a significance level of zero for regression equation, indicating that the proposed equation is appropriate for estimating BTS. Further evaluation of the suitability of the constant values and coefficients is carried out through the T-test, as shown in Table 5.

When the measured BTS varies from the predicted values determined by the models, these discrepancies are known as errors. The regression equation is not viable if the distribution of errors is not normal. Based on Fig. 4, the errors exhibit an almost normal distribution, indicating that the proposed model is suitable for use.

### 3.8 The MFF-ANN results

In the current research, using MATLAB software and the Levenberg-Marquardt training (LMT) algorithm, one to 12 neurons by trial and error process were assessed for predicting BTS. To reach the accurate number of hidden layer neurons, different MFF-ANN with different numbers of neurons were designed. The achieved optimum MFF-ANN consists of two neurons in a hidden layer with 5 inputs such as Vp, point load index (PLI), porosity (P),

**Table 4** Proposed equation for forecasting *BTS* using MVLR

| Equation | $R^2$ | *RMSE* | *MAPE* % | *DWS* | Eq. number |
|---|---|---|---|---|---|
| $BTS = -0.131 + 0.61Vp + 0.015D - 0.082A - 0.151P + 0.04PLI$ | 0.77 | 2.89 | 1.59 | 2.26 | (11) |

**Table 5** T-test results using multivariate linear regression

| Term | Coef | T-Value | P-Value |
|---|---|---|---|
| Constant | -0.1308 | -2.58 | 0.012 |
| Vp | 0.611 | 3.66 | 0.001 |
| D | 0.015 | 0.12 | 0.909 |
| A | -0.082 | -0.70 | 0.487 |
| P | -0.151 | -1.13 | 0.262 |
| PLI | 0.040 | 0.28 | 0.781 |

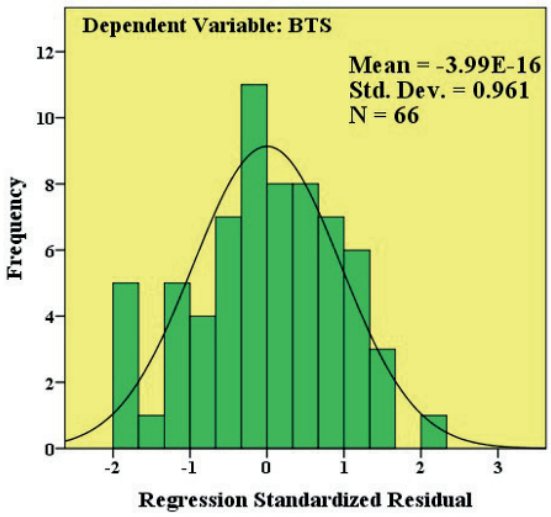


**Fig. 4** Normal histogram of the residues for model 11

density (D), water absorption (A), and BTS output. Total data were divided into groups of testing (15% all data = 10 samples), validation (15% all data = 10 samples), and training (70% all data = 46 samples). For teaching algorithms and obtaining exact weights of desired results, the training group was used. Training, validation, and test groups were chosen to fix the weights, stop the overfitting procedure, and test the MFF-ANN in predicting new data, respectively [48]. Purelin and Sigmoid were used for neuron transfer functions in the middle layer and output layer, respectively. To estimate BTS, neuron two (optimal neuron) showed the best results. Fig. 5 displays the ideal MFF-ANN used in current study.

Fig. 6 shows the MFF-ANN training status diagram. This diagram shows the amount of errors. If there is no improvement 6 consecutive times (in the Val fail part) and it goes up as well, the network training will stop. In repetitions 3 to 8 in six consecutive times no improvement is observed (Fig. 6).

The MSE trend by LMT for the best model is shown in Fig. 7. The lowest MSE in the second epochs was obtained. Results of the optimal MFF-ANN model are shown in Fig. 8.

### 3.9 The SVR Results

This study utilized the RBF function for training and testing, with 70% and 30% of the data, respectively. The optimal parameters of $\varepsilon$, $\gamma$ and $C$ were found to be 0.03, 2.13, and 48, respectively, and were used to estimate BTS. The relationship between the measured and predicted BTS using this approach is depicted in Fig. 9. Comparing the SVR results with other methods utilized in this study, it was found that the SVR method outperformed the others in terms of accuracy.

Fig. 10 illustrates the error histogram produced by implementing the SVR model.

### 3.10 Results of ANFIS for estimating BTS

The input data for modeling using ANFIS include point load index (PLI), Vp, water absorption% (A), porosity% (P), and density (D) of 66 samples in the study area and the output is

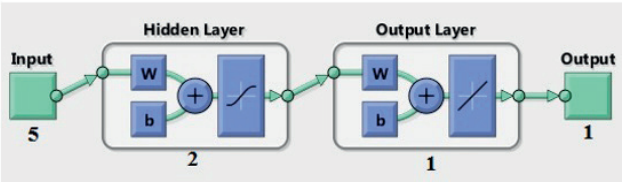


**Fig. 5** The ideal MFF-ANN used to estimate BTS

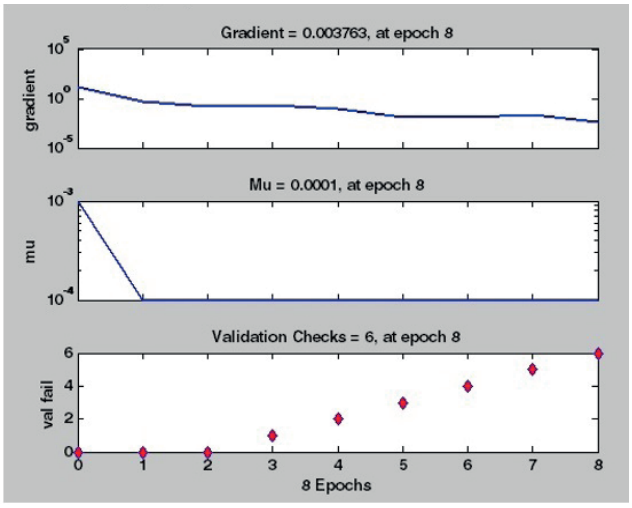


**Fig. 6** Network training status

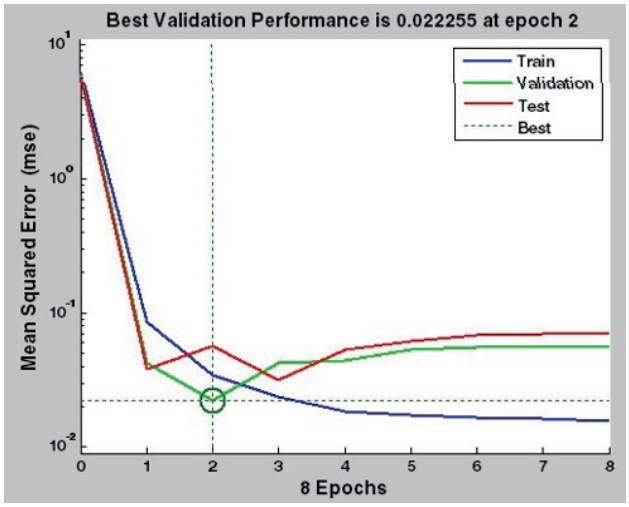


**Fig. 7** The MSE value using MFF-ANN method in the optimum model

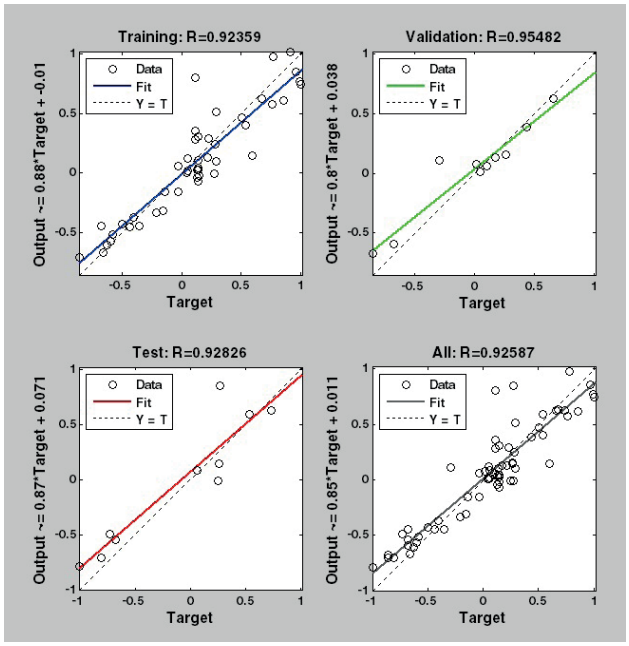


**Fig. 8** The correlation coefficients using MFF-ANN method in the optimum model

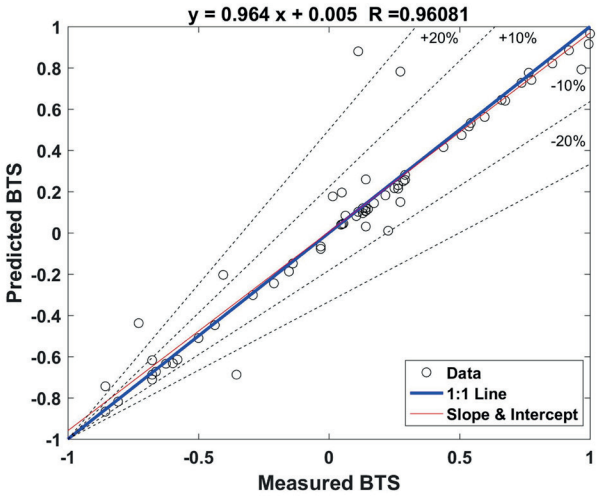


**Fig. 9** The SVR performance for predicting BTS

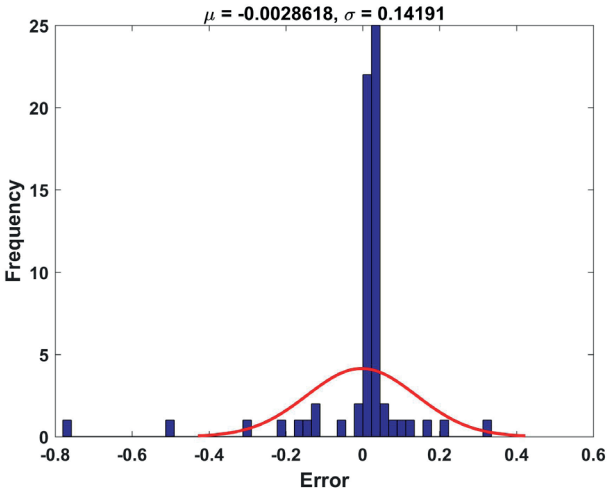


**Fig. 10** Error of SVR method in estimating BTS

**Table 6** ANFIS model summary

| | |
|---|---|
| FIS generation method | Genfis2 |
| Influence radius | 0.6 |
| Number of epochs | 300 |
| Error goal | 0 |
| Type | Sugeno |
| Rules | 3 |
| MF numbers | 3 |
| MF type for inputs | Gaussmf |
| MF type for output | Linear |

BTS. According to Table 6, the model employs three membership functions (MFs) for each variable in the input data. Gaussian functions are typically the most suitable choice for these functions, and they were also used in this study. The degree of the MFs reflects the degree of membership of a given value to the corresponding fuzzy set.

Fig. 11 depicts a diagram of the ANFIS rule viewer, which includes adaptive values for the constant output membership, for inputs 1 through 5. Each row in the diagram represents a specific rule, with the corresponding rule number displayed on the left side of Fig. 11. Each column in the diagram corresponds to a variable, with the five yellow columns representing the assumed rules and the last column representing the result of the rules.

Three Gaussian MFs were obtained for the model inputs (Fig. 12).

The utilization of the ANFIS model resulted in the development of three rules, which yielded the optimal solution compared to ANFIS models utilizing differential clustering. Fig. 13 presents the correlation of the ANFIS_s18 model.

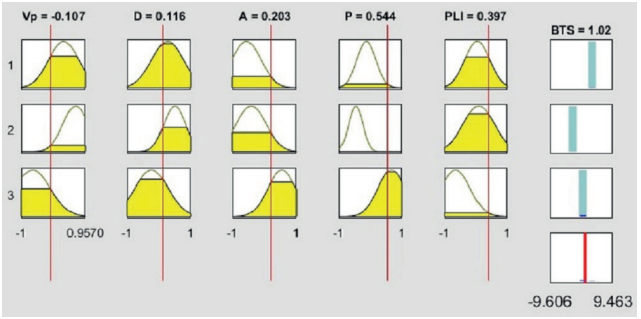


**Fig. 11** Rule displayer (there are 3 rules for predicting data relationships)

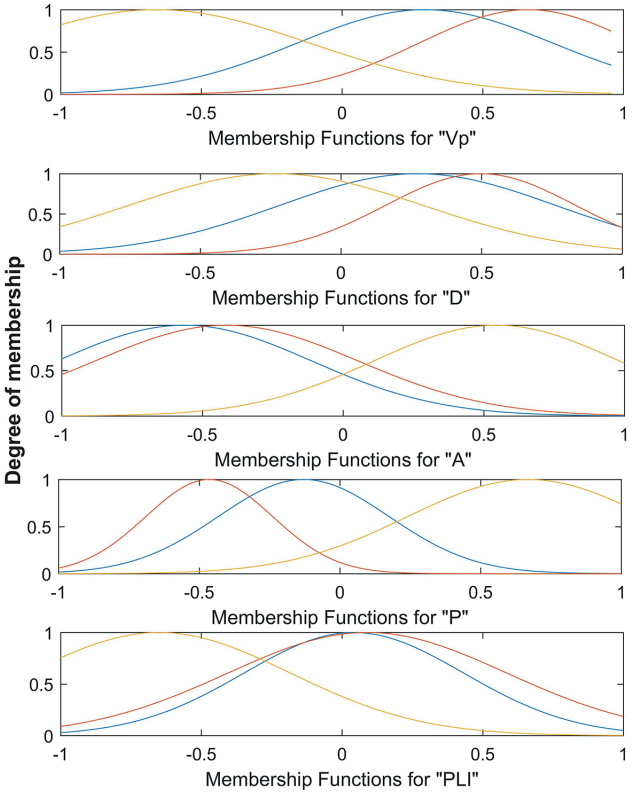


**Fig. 12** Achieved Gaussian MFs

The error value and error histogram using the ANFIS method is revealed in Fig. 14.

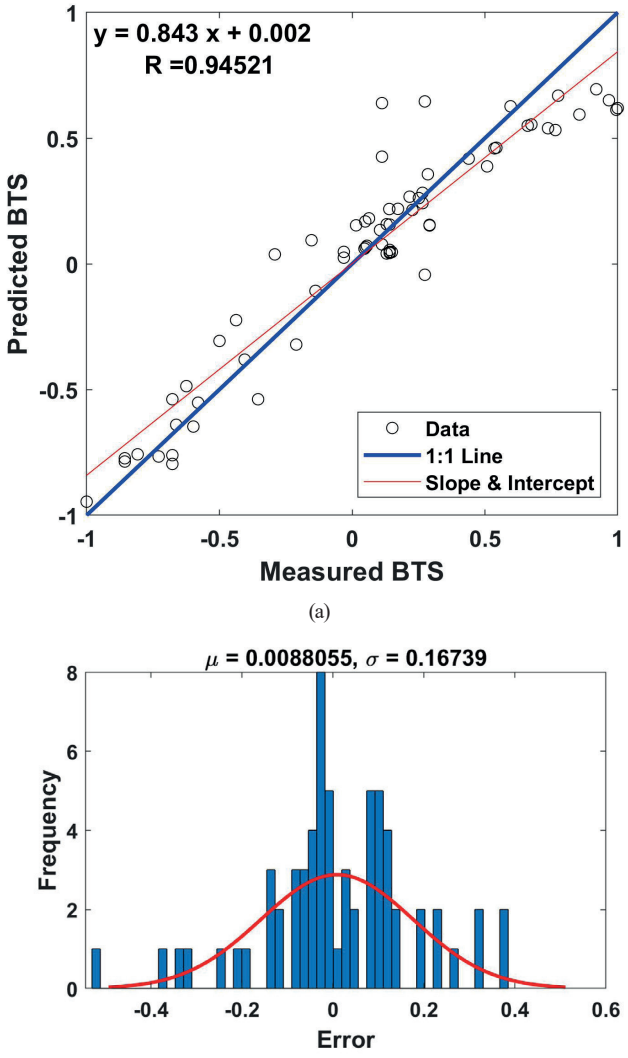


**Fig. 13** (a) Measured and predicted BTS correlation, and (b) error histogram of all data using ANFIS method

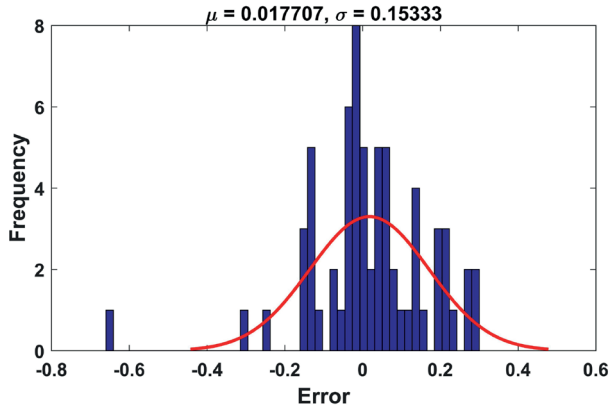


**Fig. 14** Error histogram

### 3.11 The GPR results

In this research, 70% of the data was used for training, and 30% of the data was used to test the GPR models using squared exponential kernel (SEK). Finally, the performance of the GPR models is evaluated by examining different criteria (Fig. 15). As mentioned below, the accuracy of GPR method in estimating BTS is higher than MFF-ANN and MVLR methods.

### 3.12 Comparison of used methods

Table 7 and Fig. 16 show the accuracy of the used methods for forecasting the BTS. According to the statistical criteria (i.e., R, MAPE, RMSE, and VAF), the SVR method has higher accuracy than other methods. Because SVR uses the principle of minimizing structural risk and adapting the ability of the model to existing training data [49, 50].

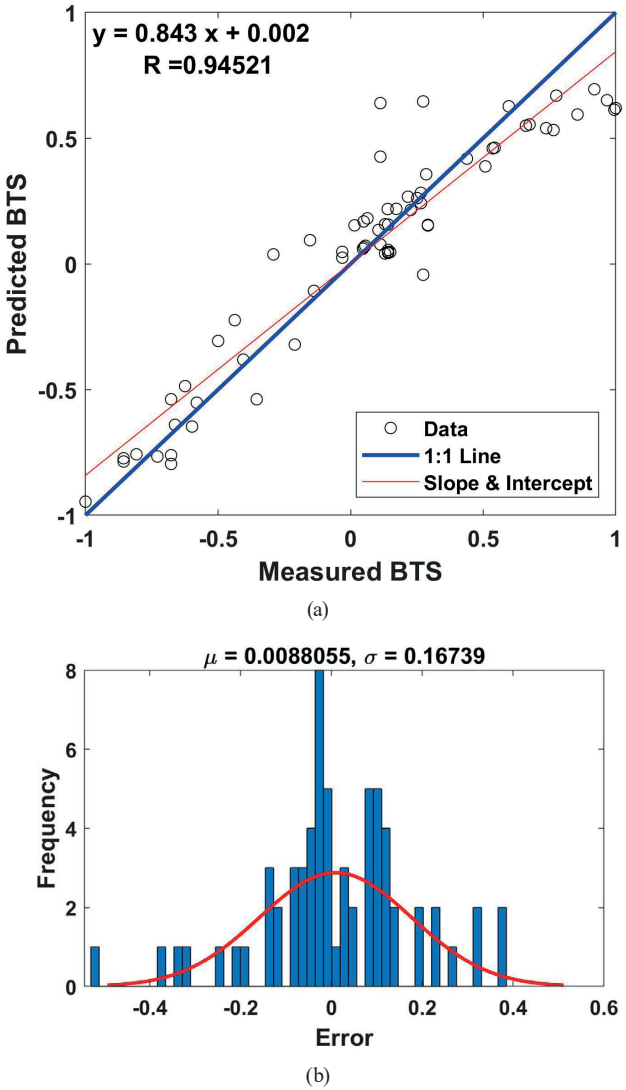


**Fig. 15** (a) Correlation coefficient, and (b) error histogram of all data set in BTS prediction by GPR

**Table 7** Precision of the used methods for test data

| Methods | R | RMSE | MAPE% | VAF% |
|---|---|---|---|---|
| SVR | 0.94 | 0.16 | 13.20 | 91.98 |
| ANFIS | 0.94 | 0.15 | 15.57 | 90.02 |
| MFF-ANN | 0.93 | 0.15 | 37.36 | 85.04 |
| MVLR | 0.91 | 1.85 | 23.67 | 82.56 |
| GPR | 0.94 | 0.17 | 18.39 | 87.72 |

The size of inputs also affects the accuracy of the methods. Considering that the number of inputs in the modeling in this research is high (5 inputs), therefore the ANFIS method works with high accuracy with a very slight difference after the SVR method. Based on the correlation coefficient, all methods (R > 91%) have very high accuracy for estimating the BTS.

The average predicted BTS from all 5 methods is 6.62 MPa. The mean percentage of predicted BTS changes obtained from all five methods compared to the measured value is -1.34%, which shows less than 5% changes.

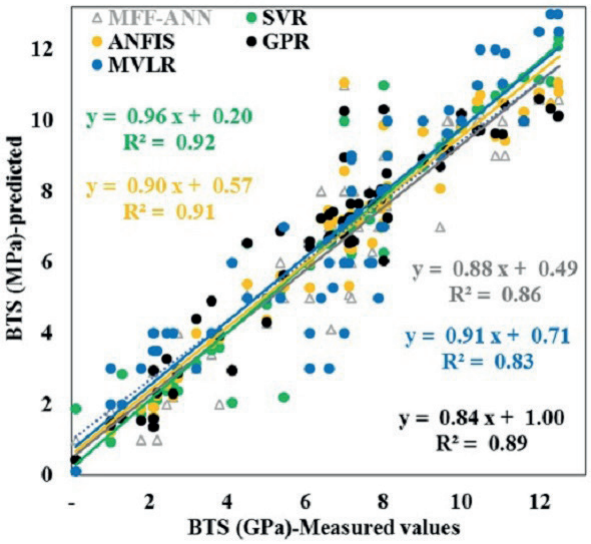


**Fig. 16** Precision of used methods for forecasting BTS

## 4 Conclusions

The construction of engineering structures including highways on the rocks is considerably controlled by the tensile strength. Tensile strength prediction based on physical and mineralogical properties can help to reduce the costs of sample preparation and testing to measure this parameter. In this study, after investigating the texture effect on geo-mechanical properties, several models for estimating BTS were established via MFF-ANN, GPR, ANFIS, SVR, and simple and multivariate regression methods.

Limestone specimens exhibit a range of textures, from mudstone to grainstone. The texture effect on 43 samples of limestone and argillaceous limestone showed that by changing the texture from mudstone to grainstone, point load index (PLI), density, Brazilian tensile strength (BTS), and Vp of the samples increased, and porosity and water absorption decreased.

The inputs for developing BTS predictor models included Vp, porosity, density, PLI, and water absorption percentage. To evaluate the performance of the models, various criteria such as $R^2$, RMSE, MAPE, DWS, ANOVA, T-test, and VAF were employed. Based on these criteria, the accuracy of MFF-ANN, GPR, ANFIS, and MVLR to estimate BTS was found to be inferior to that of SVR. Results from SVR using radial basis kernel function indicated R value of 0.96 for BTS. The analysis of all model criteria using simple and multiple regression confirmed the usability of the equation.

Regarding the use of developed relationships, it should be noted that the relationships provided by different researchers depend on the type of rock, the range of values (each relationship is given for a certain range of values), the microscopic characteristics of the samples, the conditions and how the experiment is performed. Each relationship applies to a particular region. Therefore, if any of these relationships are used, the above points should be considered.

## References

[1] Efe, T., Demirdag, S., Tufekci, K., Sengun, N., Altindag, R. "Estimating the direct tensile strength of rocks from indirect tests", Arabian Journal of Geosciences, 14, 1343, 2021. https://doi.org/10.1007/s12517-021-07539-9

[2] Parsajoo, M., Armaghani, D. J., Mohammed, A. S., Khari, M., Jahandari, S. "Tensile strength prediction of rock material using non-destructive tests: A comparative intelligent study", Transportation Geotechnics, 31, 100652, 2021. https://doi.org/10.1016/j.trgeo.2021.100652

[3] Gurocak, Z., Solanki, P., Alemdag, S., Zaman, M. M. "New considerations for empirical estimation of tensile strength of rocks", Engineering Geology, 146, pp. 1–8, 2012. https://doi.org/10.1016/j.enggeo.2012.06.005

[4] Harandizadeh, H., Armaghani, D. J., Mohamad, E. T. "Development of fuzzy-GMDH model optimized by GSA to predict rock tensile strength based on experimental datasets", Neural Computing and Applications, 32, pp. 14047–14067, 2020. https://doi.org/10.1007/s00521-020-04803-z

[5] Ren, C., Yu, J., Liu, S., Yao, W., Zhu, Y., Liu, X. "A Plastic Strain-Induced Damage Model of Porous Rock Suitable for Different Stress Paths", Rock Mechanics and Rock Engineering, 55, pp. 1887–1906, 2022.
https://doi.org/10.1007/s00603-022-02775-1

[6] Peng, J., Xu, C., Dai, B., Sun, L., Feng, J., Huang, Q. "Numerical Investigation of Brittleness Effect on Strength and Microcracking Behavior of Crystalline Rock", International Journal of Geomechanics, 22(10), pp. 4022178, 2022.
https://doi.org/10.1061/(ASCE)GM.1943-5622.0002529

[7] Rastegarnia, A., Lashkaripour, G. R., Ghafoori, M., Farrokhad, S. S. "Assessment of the engineering geological characteristics of the Bazoft dam site, SW Iran", Quarterly Journal of Engineering Geology and Hydrogeology, 52(3), pp. 360–374, 2019.
https://doi.org/10.1144/qjegh2017-042

[8] Arman, H. "Correlation of uniaxial compressive strength with indirect tensile strength (Brazilian) and 2nd cycle of slake durability index for evaporitic rocks", Geotechnical and Geological Engineering, 39(2), pp. 1583–1590, 2021.
https://doi.org/10.1007/s10706-020-01578-x

[9] Armaghani, D. J., Monjezi, M., Murlidhar, B. R., Mohamad, E. T. "Indirect estimation of rock tensile strength based on simple and multiple regression analyses", Proceedings of INDOROCK 2016, 6th Indian Rock Conference, Mumbai, India, 2016, pp. 593–603. [Rep.] Available at: http://repository.iitr.ac.in/handle/123456789/27710

[10] Mahdiyar, A., Armaghani, D. J., Marto, A., Mehrbakhsh, N., Ismail, S. "Rock tensile strength prediction using empirical and soft computing approaches", Bulletin of Engineering Geology and the Environment, 78, pp. 4519–4531, 2019.
https://doi.org/10.1007/s10064-018-1405-4

[11] Huang, L., Asteris, P. G., Koopialipoor, M., Armaghani, D. J., Tahir, M. M. "Invasive weed optimization technique-based ANN to the prediction of rock tensile strength", Applied Sciences, 9(24), 5372, 2019.
https://doi.org/10.3390/app9245372

[12] Baykasoğlu, A., Güllü, H., Çanakçı, H., Özbakır, L. "Prediction of compressive and tensile strength of limestone via genetic programming", Expert Systems with Applications, 35(1–2), pp. 111–123, 2008.
https://doi.org/10.1016/j.eswa.2007.06.006

[13] Singh, P. K., Tripathy, A., Kainthola, A., Mahanta, B., Sing, V., Singh, T. N. "Indirect estimation of compressive and shear strength from simple index tests", Engineering with Computer, 33, pp. 1–11, 2017.
https://doi.org/10.1007/s00366-016-0451-4

[14] Fattahi, H., Hasanipanah, M. "An indirect measurement of rock tensile strength through optimized relevance vector regression models, a case study", Environmental Earth Sciences, 80(22), 748, 2021.
https://doi.org/10.1007/s12665-021-10049-2

[15] Hasanipanah, M., Zhang, W., Armaghani, D. J., Rad, H. N. "The potential application of a new intelligent based approach in predicting the tensile strength of rock", IEEE Access, 8, pp. 57148–57157, 2020.
https://doi.org/10.1109/ACCESS.2020.2980623

[16] Dao, D. V., Adeli, H., Ly, H.-B., Le, L. M., Le, V. M., Le, T.-T., Pham, B. T. "A sensitivity and robustness analysis of GPR and ANN for high-performance concrete compressive strength prediction using a Monte Carlo simulation", Sustainability, 12(3), 830, 2020.
https://doi.org/10.3390/su12030830

[17] Armaghani, D. J., Asteris, P. G., Askarian, B., Hasanipanah, M., Tarinejad, R., Huynh, V. V. "Examining hybrid and single SVM models with different kernels to predict rock brittleness", Sustainability, 12(6), 2229, 2020.
https://doi.org/10.3390/su12062229

[18] Mahmoodzadeh, A., Mohammadi, M., Ali, H. F. H., Abdulhamid, S. N., Ibrahim, H. H., Noori, K. M. G. "Dynamic prediction models of rock quality designation in tunneling projects", Transportation Geotechnics, 27, 100497, 2021.
https://doi.org/10.1016/j.trgeo.2020.100497

[19] Lawal, A. I., Kwon, S., Aladejare, A. E., Oniyide, G. O. "Prediction of the static and dynamic mechanical properties of sedimentary rock using soft computing methods", Geomechanics and Engineering, 28(3), pp. 313–324, 2022.
https://doi.org/10.12989/gae.2022.28.3.313

[20] Acar, M. C., Kaya, B. "Models to estimate the elastic modulus of weak rocks based on least square support vector machine", Arabian Journal of Geosciences, 13(14), 590, 2020.
https://doi.org/10.1007/s12517-020-05566-6

[21] Mishra, D. A., Basu, A. "Use of the block punch test to predict the compressive and tensile strengths of rocks", International Journal of Rock Mechanics and Mining Sciences, 51, pp. 119–127, 2012.
https://doi.org/10.1016/j.ijrmms.2012.01.016

[22] Karaman, K., Kesimal, A., Ersoy, H. "A comparative assessment of indirect methods for estimating the uniaxial compressive and tensile strength of rocks", Arabian Journal of Geosciences, 8(4), pp. 2393–2403, 2015.
https://doi.org/10.1007/s12517-014-1384-0

[23] Yilmaz, I. "Use of the core strangle test for tensile strength estimation and rock mass classification", International Journal of Rock Mechanics and Mining Sciences, 47, pp. 845–850, 2010.
https://doi.org/10.1016/j.ijrmms.2010.03.003

[24] Khajevand, R., Fereidooni, D. "Utilization of the point load and block punch strengths to predict the mechanical properties of several rock samples using regression analysis methods", Innovative Infrastructure Solution, 4(1), 15, 2019.
https://doi.org/10.1007/s41062-019-0201-8

[25] Kılıç, A., Teymen, A. "Determination of mechanical properties of rocks using simple methods", Bulletin of Engineering Geology and the Environment, 67(2), pp. 237–244, 2008.
https://doi.org/10.1007/s10064-008-0128-3

[26] Karakul, H., Ulusay, R. "Empirical correlations for predicting strength properties of rocks from P-wave velocity under different degrees of saturation", Rock Mechanic and Rock Engineering, 46(5), pp. 981–999, 2013.
https://doi.org/10.1007/s00603-012-0353-8

[27] Brown, E. T. (ed.) "Rock Characterization, Testing & Monitoring: ISRM Suggested Methods", Pergamon Press, 1981. ISBN: 0080273092

[28] ASTM "D3967 Standard test method for splitting tensile strength of intact rock core specimens", ASTM International, West Conshohocken, PA, USA, 1996.
https://doi.org/10.1520/D3967-95A

[29] ASTM "D5731-16 Standard Test Method for Determination of the Point Load Strength Index of Rock and Application to Rock Strength Classifications", ASTM International, West Conshohocken, PA, USA, 1996.
https://doi.org/10.1520/D5731-16

[30] Folk, R. L. "Petrology of Sedimentary Rocks", Hemphill Publishing, 1974.

[31] Dunham, R. J. "Classification of carbonate rocks according to depositional textures", In: Ham, W. E. Classification of Carbonate Rocks - A Symposium, American Association of Petroleum Geologists, 1962, pp. 108–121. ISBN: 0891812768

[32] Zhan, C., Dai, Z., Yang, Z., Zhang, X., Ma, Z., Thanh, H. V., Soltanian, M. R. "Subsurface sedimentary structure identification using deep learning: A review", Earth-Science Reviews, 239, 104370, 2023.
https://doi.org/10.1016/j.earscirev.2023.104370

[33] Zhou, G., Zhang, R., Huang, S. "Generalized Buffering Algorithm", IEEE Access", 9, pp. 27140–27157, 2021.
https://doi.org/10.1109/ACCESS.2021.3057719

[34] Kazemzadeh, E., Azar, S. Z. "Sales concentration index in the Iranian car market", Industrija, 43(4), pp. 129–149, 2015.
https://doi.org/https://doi.org/10.5937/industrija43-8616

[35] Bieniawski, Z. T. "Point load test in geotechnical practice", Engineering Geology, 9(1), pp. 1–11, 1975.
https://doi.org/10.1016/0013-7952(75)90024-1

[36] Yang, J., Fu, L.-Y., Fu, B.-Y., Deng, W., Han, T. "Third-Order Padé Thermoelastic Constants of Solid Rocks", Journal of Geophysical Research: Solid Earth, 127(9), e2022J–e24517J, 2022.
https://doi.org/10.1029/2022JB024517

[37] Wu, Z., Xu, J., Li, Y., Wang, S. "Disturbed State Concept–Based Model for the Uniaxial Strain-Softening Behavior of Fiber-Reinforced Soil", International Journal of Geomechanics, 22(7), 4022092, 2022.
https://doi.org/10.1061/(ASCE)GM.1943-5622.0002415

[38] Li, X., Du, C., Wang, X., Zhang, J. "Quantitative Determination of High-Order Crack Fabric in Rock Plane", Rock Mechanics and Rock Engineering, 2023.
https://doi.org/10.1007/s00603-023-03319-x

[39] Xu, Z., Wang, Y., Jiang, S., Fang, C., Liu, L., Wu, K., Luo, Q., Li, X., Chen, Y. "Impact of input, preservation and dilution on organic matter enrichment in lacustrine rift basin: A case study of lacustrine shale in Dehui Depression of Songliao Basin, NE China", Marine and Petroleum Geology, 135, 105386, 2022.
https://doi.org/10.1016/j.marpetgeo.2021.105386

[40] Liu, C., Peng, Z., Cui, J., Huang, X., Li, Y., Chen, W. "Development of crack and damage in shield tunnel lining under seismic loading: Refined 3D finite element modeling and analyses", Thin-Walled Structures, 185, 110647, 2023.
https://doi.org/10.1016/j.tws.2023.110647

[41] Jia, S., Dai, Z., Zhou, Z., Ling, H., Yang, Z., Qi, L., Wang, Z., Zhang, X., Thanh, H. V., Soltanian, M. R. "Upscaling dispersivity for conservative solute transport in naturally fractured media", Water Research, 235, 119844, 2023.
https://doi.org/10.1016/j.watres.2023.119844

[42] Xu, J., Lan, W., Ren, C., Zhou, X., Wang, S., Yuan, J. "Modeling of coupled transfer of water, heat and solute in saline loess considering sodium sulfate crystallization", Cold Regions Science and Technology, 189, 103335, 2021.
https://doi.org/10.1016/j.coldregions.2021.103335

[43] Xiao, D., Hu, Y., Wang, Y., Deng, H., Zhang, J., Tang, B., Xi, J., Tang, S., Li, G. "Wellbore cooling and heat energy utilization method for deep shale gas horizontal well drilling", Applied Thermal Engineering, 213, 118684, 2022.
https://doi.org/10.1016/j.applthermaleng.2022.118684

[44] Xu, Z., Li, X., Li, J., Xue, Y., Jiang, S., ..., Sun, Q. "Characteristics of Source Rocks and Genetic Origins of Natural Gas in Deep Formations, Gudian Depression, Songliao Basin, NE China", ACS Earth and Space Chemistry, 6(7), pp. 1750–1771, 2022.
https://doi.org/10.1016/10.1021/acsearthspacechem.2c00065

[45] Yu, J., Zhu, Y., Yao, W., Liu, X., Ren, C., Cai, Y., Tang, X. "Stress relaxation behaviour of marble under cyclic weak disturbance and confining pressures", Measurement, 182, 109777, 2021.
https://doi.org/10.1016/j.measurement.2021.109777

[46] Zhang, X., Ma, F., Dai, Z., Wang, J., Chen, L., Ling, H., "Soltanian, M. R. "Radionuclide transport in multi-scale fractured rocks: A review", Journal of Hazardous Materials, 424(C), 127550, 2022.
https://doi.org/10.1016/j.jhazmat.2021.127550

[47] Zhang, X., Wang, Z., Reimus, P., Ma, F., Soltanian, M. R., Xing, B., Zang, J., Wang, Y., Dai, Z. "Plutonium reactive transport in fractured granite: Multi-species experiments and simulations", Water Research, 224, 119068, 2022.
https://doi.org/10.1016/j.watres.2022.119068

[48] Rastegarnia, A., Lashkaripour, G. R., Sharifi Teshnizi, E., Ghafoori, M. "Evaluation of engineering characteristics and estimation of static properties of clay-bearing rocks", Environmental Earth Sciences, 80(18), 621, 2021.
https://doi.org/10.1007/s12665-021-09914-x

[49] Khajehzadeh, M., Keawsawasvong, S., Sarir, P., Khailany, D. K. "Seismic Analysis of Earth Slope Using a Novel Sequential Hybrid Optimization Algorithm", Periodica Polytechnica Civil Engineering, 66(2), pp. 355–366, 2022.
https://doi.org/10.3311/PPci.19356

[50] Zeng, X., Khajehzadeh, M., Iraji, A. Keawsawasvong, S. "Probabilistic Slope Stability Evaluation Using Hybrid Metaheuristic Approach", Periodica Polytechnica Civil Engineering, 66(4), pp. 1309–1322, 2022,
https://doi.org/10.3311/PPci.20502